Available online at www.sciencedirect.com
ScienceDirect
Trans. Nonferrous Met. Soc. China 34(2024) 669−680
Transactions of Nonferrous Metals Society of China
www.tnmsc.cn

Acidic leaching kinetics study on vanadium from magnesiation-roasted vanadium slag

Jie CHENG[1], Hong-yi LI[1,2], Dong HAI[1], Xin-mian CHEN[1], Jiang DIAO[1,2], Bing XIE[1]

1. College of Materials Science and Engineering, Chongqing University, Chongqing 400044, China;
2. National Engineering Research Center for Magnesium Alloys, Chongqing University, Chongqing 400044, China

Received 28 September 2022; accepted 13 March 2023

Abstract: In order to promote the industrial application of the magnesiation roasting–acid leaching method, the acidic leaching kinetics of vanadium from magnesiation-roasted vanadium slag was investigated. By combination of XRD, XPS, and SEM, it was revealed that $MgSiO_3$ and most vanadates consumed acid sharply to produce SiO_2 and V(V)-containing vanadyl in the initial 10 min. The variation of vanadium extraction efficiency with leaching time was studied to establish the kinetic models for leaching. Results indicated two distinct stages in the leaching process and the kinetics of both stages followed the shrinking core model. The leaching rate in 0−10 min was controlled by both solid product layer diffusion and chemical reactions, while the leaching rate in 10−30 min was controlled only by chemical reactions. Therefore, it is essential to accelerate the mass transfer in initial 10 min and accurately control the temperature in the following 20 min during leaching.

Key words: leaching kinetics; magnesiation roasting; acid leaching; vanadium extraction; vanadium slag

1 Introduction

Vanadium is a strategic metal [1−3] that has widespread applications in national defense, chemical and metallurgical engineering due to its special properties [4−8]. For vanadium extraction, the vanadium slag obtained from the V−Ti magnetite ores is the major raw material [1,9,10]. In the vanadium slag, V exists as V(III) and concentrates in the spinel phase [11−13]. The V(III)-bearing spinels transform into leachable vanadates (V(V)) during the oxidative roasting−leaching process of vanadium slag for vanadium extraction [14−17].

At present, the common methods of vanadium extraction from vanadium slag are the sodium roasting–water leaching method and the calcification roasting−acid leaching method [18]. The sodium roasting process produces harmful gases, including sulfur dioxide, sulfur trioxide, chlorine, and hydrogen chloride, which are harmful to the environment [19,20]. For the calcification roasting−acid leaching process, the leaching residues contain high content of calcium sulfate, which makes their iron resource difficult to be utilized [21,22]. In order to solve the problems associated with methods above, our group has proposed a green method of magnesiation roasting–acid leaching to selectively extract vanadium and make the associated resources utilizable [6]. To put forward the industrial application of this green vanadium extraction method, it is essential to study the acidic leaching kinetics of vanadium from the magnesiation-roasted vanadium slag in order to maintain the high leaching efficiency at a large reaction scale.

Many researchers have studied the leaching kinetics of vanadium from vanadium slag roasted with non-Mg additives. AARABI-KARASGANI

Corresponding author: Hong-yi LI, Tel: +86-23-65102469, Fax: +86-23-65127306, E-mail: hongyi.li@cqu.edu.cn
DOI: 10.1016/S1003-6326(23)66426-X

et al [23] studied the acid leaching kinetics of vanadium from alkaline-roasted Linz-Donawitz (LD) converter slag and found that the leaching kinetics at low temperature was controlled by chemical reactions in the whole leaching process. PENG et al [24] reported the leaching kinetics of vanadium from calcification-roasted vanadium slag in acidic medium, and found that the leaching process followed the shrinking core model (SCM) and was mainly controlled by the solid product layer diffusion. LI et al [25] investigated the leaching kinetics of vanadium in non-salt roasted vanadium slag with ammonium bicarbonate as the leaching agent. It was found that the ammonium bicarbonate leaching process followed the SCM and the leaching process can be divided into two distinct stages. The first stage, which is in the time range of initial 30 min, was controlled by the solid product diffusion and the second stage, which is in the time range of 30−150 min, was controlled by the surface chemical reactions. All these studies investigated the kinetics of leaching process in which the solid products were produced during leaching and they could wrap the vanadates and inhibit the vanadium dissolution. However, in the case of the acid leaching process of magnesiation-roasted vanadium slag, all products of vanadium leaching reactions are soluble, whose leaching kinetics cannot be directly identical to the kinetic behavior mentioned in above cases.

Therefore, this study focused on the leaching kinetics of vanadium in the magnesiation-roasted slag, including the leaching mechanism and the kinetic models. Via combination of XRD, XPS, FT-IR and SEM, the leaching mechanism of vanadium was systematically investigated. The influences of liquid/solid (L/S) ratio, leaching temperature, and pH value on the vanadium leaching kinetics were studied to explore the rate-controlling step and the kinetic models.

2 Experimental

2.1 Materials and characterization

The vanadium slag was supplied by the Pan Steel Company, China. The chemical composition of the vanadium slag (Table 1) was determined using X-ray fluorescence (XRF, Shimadzu XRF−1800, Japan) technique. The phase compositions of the vanadium slag (Fig. 1), the roasted slag and the leaching residues were determined via powder X-ray diffraction (XRD, Rigaku D/MAX 2500PC, Japan) analysis using Cu K_α radiation. In Fig. 1, the major phases present are $(Fe,Mg)V_2O_4$ spinels and Fe_2SiO_4 fayalite, while $MnFe_2O_4$, Mg_2TiO_4 spinels, $Ca(Ti,Mg,Al)(Si,Al)_2O_6$ pyroxenes, and Fe_3O_4 are the minor phases in the vanadium slag. The elemental vanadium concentrations in the leaching liquid were analyzed using inductively coupled plasma-atomic emission spectrometry (ICP-OES, Optima 8000, USA). X-ray photoelectron spectroscopy (XPS, ThermoFisher ESCALAB250Xi, USA) was utilized to characterize the chemical valences of major elements in the vanadium slag, the magnesiation-roasted slag, and the leaching residue. Scanning electron microscopy (SEM, TESCAN MIRA LMS, Czech) equipped with energy-dispersive X-ray spectrometry (Xplore 30) was used to conduct the microscopic observation of the vanadium slag (Fig. 2), the magnesiation-roasted slag, and the leaching residues. As shown in Fig. 2, V and Ti are distributed in the same areas while Si is distributed in the surrounding areas, which is in accordance with the spinel phase containing V and Ti and the fayalite phase containing Si as indicated by the XRD pattern in Fig. 1. The bonding information of original and roasted vanadium slags and the leaching residue was determined via FT-IR spectrometer (FT-IR, Thermo Scientific Nicolet 6700, USA).

Table 1 Chemical compositions of vanadium slag (wt.%)

FeO	SiO_2	TiO_2	V_2O_3	MnO	CaO	MgO	Al_2O_3
38.53	13.51	12.60	15.37	9.47	3.02	4.01	3.47

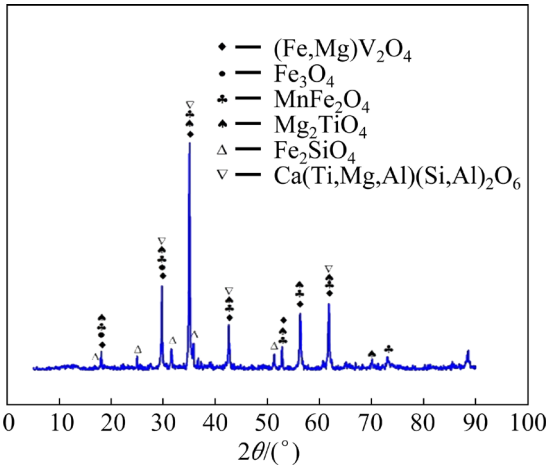

Fig. 1 XRD pattern of vanadium slag

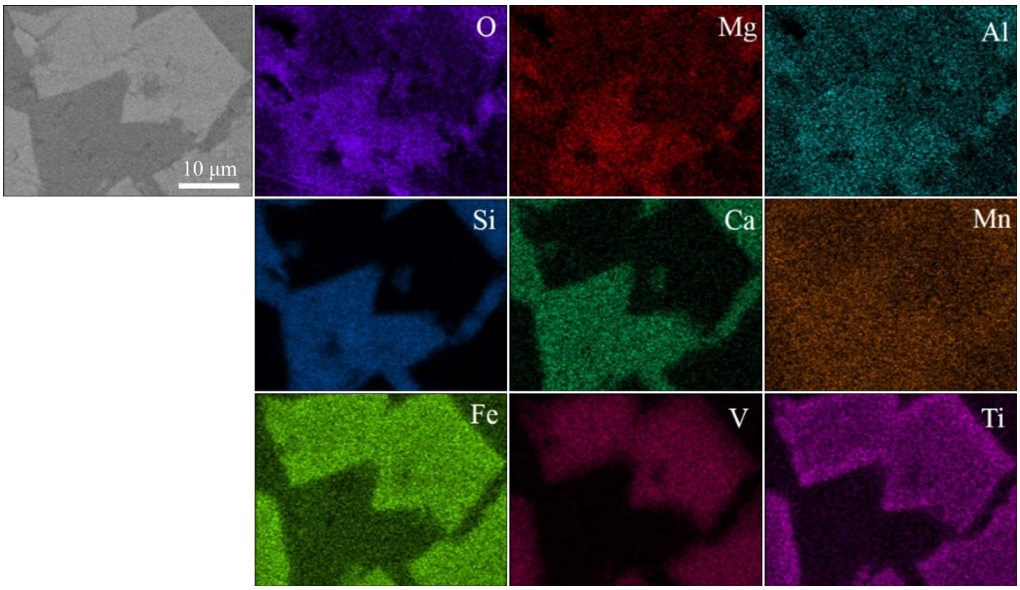

Fig. 2 SEM image of vanadium slag with element mapping

2.2 Magnesiation roasting

The vanadium slag was crushed and sieved into a particle size of <74 μm. The vanadium slag and MgO were mixed in a Mg/V molar ratio (n(Mg)/n(V)) of 0.6. The mixture was roasted in muffle furnace at 1173 K for 90 min. After roasting, the roasted sample was then air-cooled to room temperature and ground into powder.

2.3 Sulfuric acid leaching

The magnesiation-roasted slag was leached for 0−30 min using sulfuric acid in a magnetically stirred water bath with a liquid/solid (L/S) ratio of (5−8) (mL/g) and solution pH of 0.5−1 at temperatures of 313−338 K and stirring speed of 200 r/min. The leaching liquid was separated from the leaching residue via filtration. The vanadium extraction efficiency was calculated according to Eq. (1):

$$\eta=(cV/m)\times100\% \quad (1)$$

where η is the extraction efficiency; c and V represent the vanadium concentration and volume of the leaching liquid, respectively, and m denotes the vanadium mass in the magnesiation-roasted slag.

3 Results and discussion

3.1 Leaching mechanism of vanadium

3.1.1 Phase evolution

As shown in Fig. 3, the main phases in the magnesiation-roasted slag are Fe_2O_3, $Mg_2V_2O_7$, $Mn_2V_2O_7$, Fe_2TiO_5, $MgSiO_3$, $MgTi_2O_5$, and $Ca_{12}Al_{14}O_{33}$. In the process of the acid leaching, $Mg_2V_2O_7$, $Mn_2V_2O_7$, and $MgSiO_3$ in the magnesiation roasted slag reacted with sulfuric acid as follows:

$$Mg_2V_2O_7+3H_2SO_4=(VO_2)_2SO_4+2MgSO_4+3H_2O \quad (2)$$

$$Mn_2V_2O_7+3H_2SO_4=(VO_2)_2SO_4+2MnSO_4+3H_2O \quad (3)$$

$$MgSiO_3+H_2SO_4=H_2SiO_3+MgSO_4 \quad (4)$$

Figure 3 showed the XRD patterns of the roasted slags leached at 0−30 min. After leaching for 10 min, the partial diffraction peaks of $Mg_2V_2O_7$ and $Mn_2V_2O_7$ disappeared, indicating that most of $Mg_2V_2O_7$ and $Mn_2V_2O_7$ reacted with sulfuric acid. In addition, the diffraction peaks of $MgSiO_3$ disappeared, indicating that $MgSiO_3$ completely dissolved in sulfuric acid to form H_2SiO_3 during the acid leaching process. The diffraction peaks of H_2SiO_3 were not seen due to their low crystallinity. The diffraction peaks of SiO_2 appeared, which may be due to the aggregation of a large amount of H_2SiO_3 to form SiO_2 precipitate in the residue. When the leaching time prolonged to 30 min, the diffraction peaks of $Mg_2V_2O_7$ and $Mn_2V_2O_7$ completely disappeared, indicating that all $Mg_2V_2O_7$ and $Mn_2V_2O_7$ have reacted with sulfuric acid at this time.

3.1.2 Bonding structure change

The FT-IR spectra of the original vanadium slag, the roasted slag, and the leaching residue in the wavenumber range of 4000−400 cm^{-1} were

compared in Fig. 4. The absorption bands at 3438 and 1630 cm^{-1} can be attributed to the O—H stretching vibrations and the H—O—H bending vibrations of water molecules absorbed on the sample surface, respectively. In the original vanadium slag, the absorption bands at 480 and 584 cm^{-1} were the characteristic peaks of spinels. The absorption bands at 828, 876, 923, and 961 cm^{-1} were attributed to the vibration of [SiO_4] tetrahedra in olivine phases, and bonds at 1050 cm^{-1} was assigned to the Si—O—Si asymmetric stretching vibrations [14]. In fact, more absorption bands of spinels and olivines were expected theoretically in the wavenumber range of 4000−400 cm^{-1}. However, only partial absorption bands of spinels and olivines were observed in Fig. 4 because some lower frequency bands were consolidated in far-infrared region and others were consolidated by stronger bonds of other groups [4].

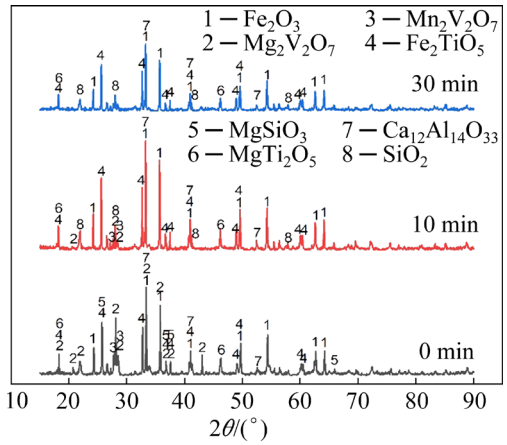

Fig. 3 XRD patterns of leaching residues at different leaching time in sulfuric acid with pH=0.5 and L/S ratio of 8:1

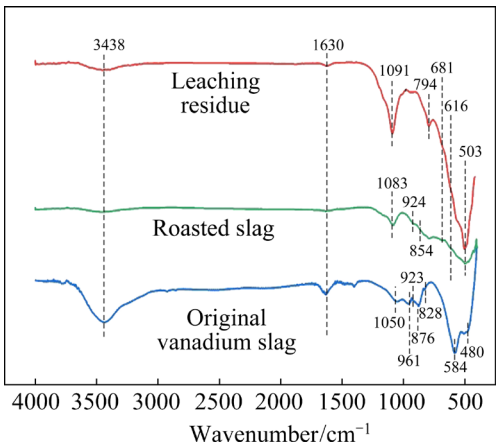

Fig. 4 FT-IR spectra of original vanadium slag, roasted slag, and leaching residue

After roasting, the absorption bands of spinels and olivines disappeared. Bands at 503 and 616 cm^{-1} were related to the M—O vibrations such as Fe—O from Fe_2O_3. The characteristic band at 681 cm^{-1} was due to different types of Ti—O—(Ti) vibrations that were related to the tetrahedrally and octahedrally coordinated Ti ion [26]. Bands at 854 and 924 cm^{-1} were assigned to the V—O stretching vibration bands of [VO_4] [4], which proved the formation of magnesium vanadates. The band at 1063 cm^{-1} shifted to 1083 cm^{-1}, indicating that there was a phase transition at this time, and the phase transition process involved Si—O—Si. Combined with Fig. 3, it was deduced that the roasting process involved the decomposition of olivine phases to generate SiO_2 which reacted further with the additive MgO to produce $MgSiO_3$.

In the leaching residue, the disappearance of bands at 854 and 924 cm^{-1} illustrated the dissolution of magnesium vanadates. The bond at 1091 cm^{-1} belonged to SiO_2 [27], indicating that the $MgSiO_3$ reacted with the sulfuric acid to produce SiO_2 during the leaching process.

3.1.3 Valence state shift

The global XPS survey of the original vanadium slag, the roasted slag, and the leaching liquid was shown in Fig. 5(a). Results demonstrated the presence of major elements in samples through the specific binding energies of different orbitals of different elements. Figures 5(b_1) and (b_2) showed the detailed XPS spectra of Fe 2p and V 2p in the original vanadium slag, respectively. For Fe, shoulders (726 and 712 eV) were observed on the major peaks at 723.5 and 710.4 eV, respectively. The 710.4 and 723.5 eV signals corresponded to Fe^{2+} [28], and the 712 and 726 eV signals corresponded to Fe^{3+} [29], which indicated that Fe^{2+} and Fe^{3+}coexisted in the original vanadium slag with Fe(II) as the major chemical valence of Fe. For V, the 516.8 and 515.9 eV signals were attributed to the V $2p_{3/2}$ of V^{3+} [30], which indicated that the V element in the original vanadium slag existed in the form of V^{3+}. After roasting, only the signals of Fe^{3+} and V^{5+} can be observed in Figs. 5(c_1) and (c_2), indicating that all the Fe^{2+} and V^{3+} ions were oxidized to Fe^{3+} and V^{5+}, respectively, which were consistent with the previous XRD results. After sulfuric acid leaching, V in the leaching liquid presented in the form of V^{5+} (Fig. 5(d_2)). However, the Fe was hardly detected in the leaching liquid,

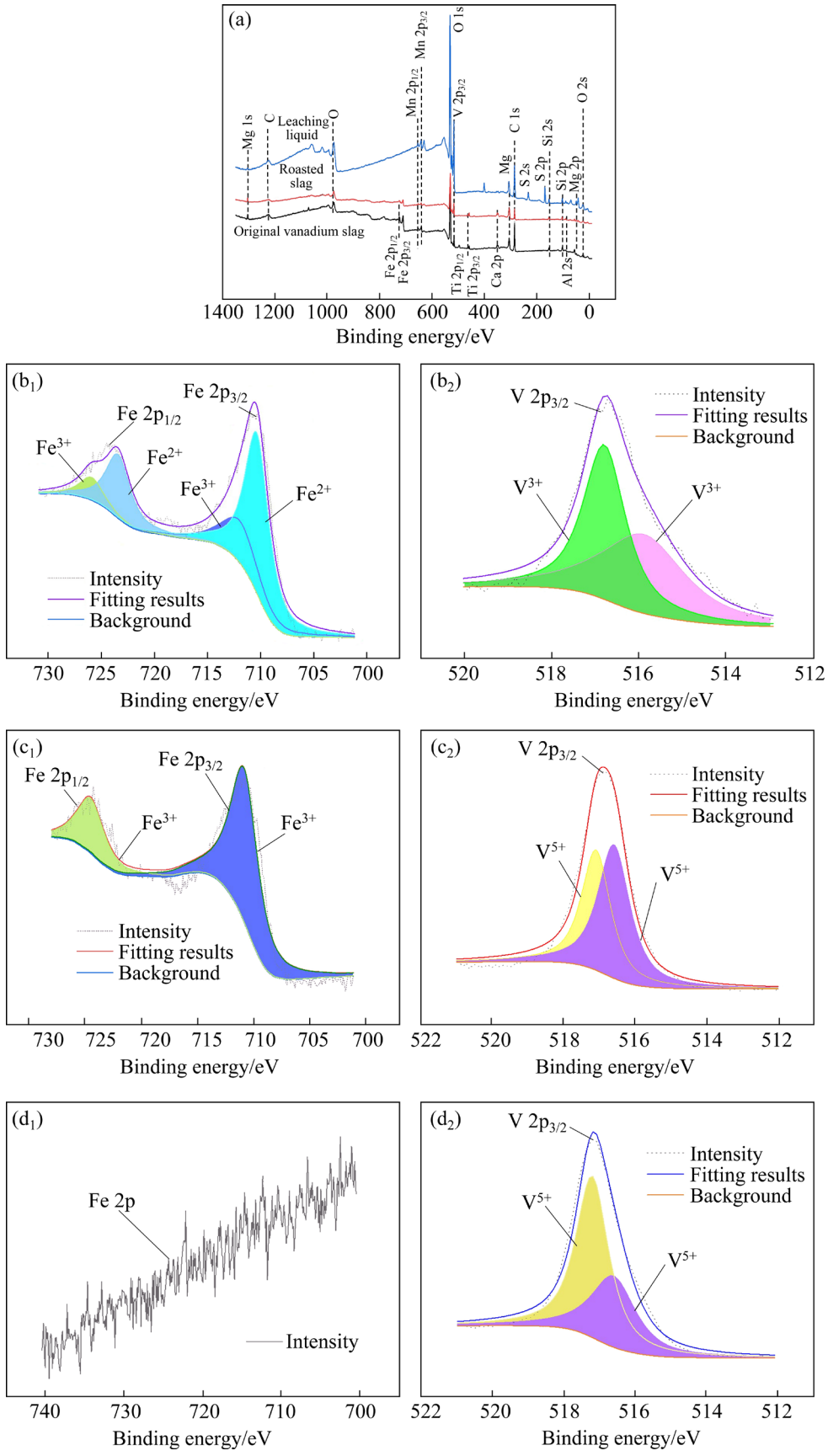

Fig. 5 XPS spectra of original vanadium slag, roasted slag, and leaching residue: (a) Global XPS; (b_1, b_2, c_1, c_2, d_1, d_2) Chemical valences of Fe and V in original vanadium slag (b_1, b_2), roasted slag (c_1, c_2), and leaching liquid (d_1, d_2)

which was because Fe in the roasted slag mainly existed as acid-insoluble products, which maintained in the leaching residue during the leaching process (Fig. 5(d_1)).

3.1.4 Microstructure change

The SEM images of the magnesiation-roasted slag with energy dispersive spectrometer (EDS) point scanning were shown in Fig. 6(a). Compared with Fig. 2, the surface morphology of the magnesiation-roasted slag undergone great changes, indicating that the additive MgO reacted strongly with the vanadium slag during the magnesiation roasting process. In addition, the point scanning results showed that the major phases in the regular area (the area where the vanadium spinels were located in the vanadium slag) were vanadates, indicating that the vanadium spinels were transformed into vanadates during the magnesiation roasting process. After leaching, the surface morphology of the leaching residue (Fig. 6(b)) changed significantly compared with Fig. 6(a). The spot scanning results showed that the vanadium content in the region corresponding to vanadates was low, indicating that the vanadates were dissolved in the sulfuric acid, which was in accordance with the XRD results in Fig. 3.

3.2 Influences of leaching conditions on leaching kinetics

The dependence of vanadium leaching kinetics on L/S ratio, pH value of leaching reagent, and leaching temperature was systematically investigated.

The influence of L/S ratio on vanadium leaching kinetics was illustrated in Fig. 7(a). As shown in Fig. 7(a), there were two distinct stages in the leaching process at all L/S ratios, but the stage ranges were different. At low L/S ratio of 5:1, the vanadium leaching efficiency increased sharply in

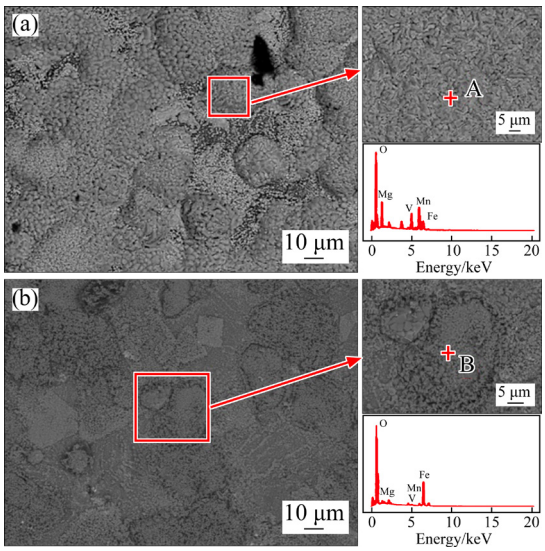

Fig. 6 SEM images of roasted slag before (a) and after (b) leaching with EDS point scanning (Leaching condition: sulfuric acid solution pH=0.5, leaching time of 30 min, and L/S ratio of 8:1)

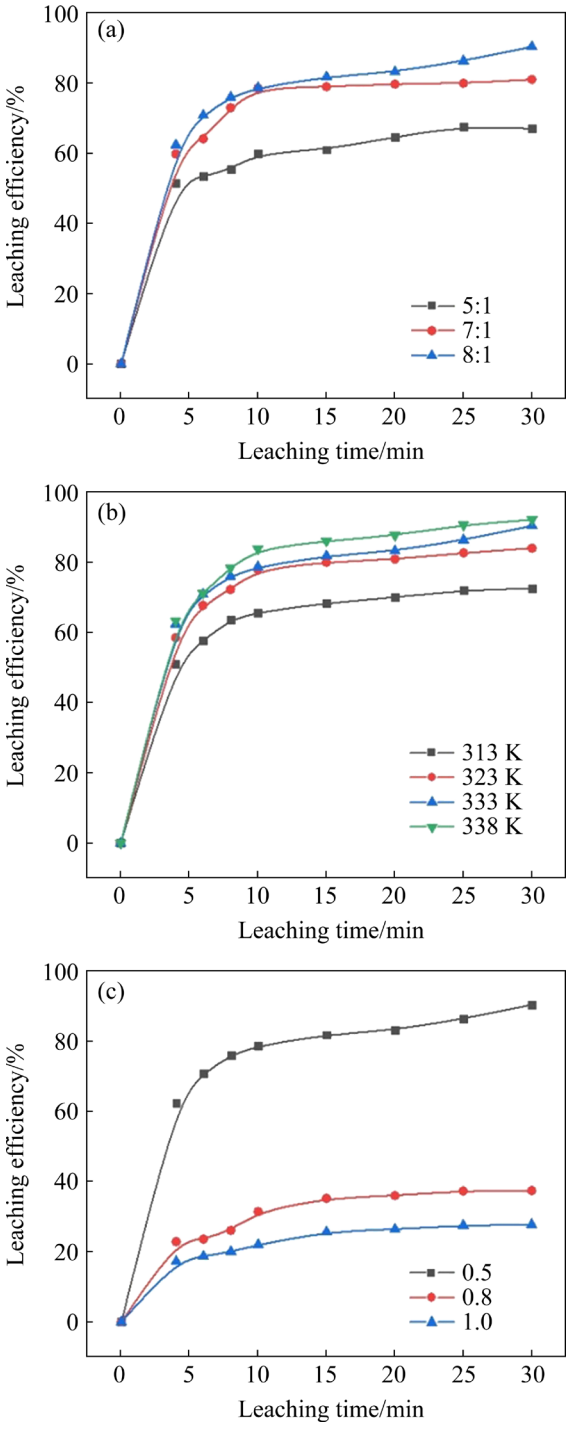

Fig. 7 Effects of leaching conditions on vanadium leaching kinetics: (a) L/S ratio; (b) Leaching temperature; (c) pH value

the initial 3 min, and reached a plateau at 5 min, after which the vanadium leaching efficiency increased slowly. When the L/S ratio increased to 7:1, the vanadium leaching efficiency increased more rapidly in the initial 10 min and then reached a plateau of leaching efficiency higher than that at L/S ratio of 5:1. As the L/S ratio increased to 8:1, both the increase rate and the plateau value of vanadium leaching efficiency increased further, with the leaching time of 10 min as the boundary for two leaching stages.

The influence of leaching temperature on vanadium leaching kinetics was demonstrated in Fig. 7(b). As the leaching temperature increased from 313 to 333 K, the increase rate and plateau value of vanadium leaching efficiency increased significantly. However, when the leaching temperature increased further to 338 K, the increase rates of leaching efficiency in both stages (0−10 min and 10−30 min) were almost the same compared to the case of 333 K; the maximal value of leaching efficiency only increased slightly. Thus, in order to save energy, 333 K was the optimal leaching temperature in this study.

The pH value of sulfuric acid (leaching reagent) had significant influence on the vanadium leaching kinetics. As shown in Fig. 7(c), when the pH value of leaching reagent decreased from 1.0 to 0.8, the increase rate and plateau value of vanadium leaching efficiency increased obviously. When the pH value decreased further to 0.5, the leaching efficiency increased much more rapidly in the initial 10 min and slightly rapidly in 10−30 min; the maximal leaching efficiency was almost 3 times that at higher pH values. This indicated that the increase in sulfuric acid concentration largely promoted the leaching kinetics of vanadium.

3.3 Kinetic model of leaching process

The pseudo-first order model, pseudo-second order model, and SCM were used for kinetic analysis [31]. Among them, the SCM showed the highest fitting coefficient. In SCM, the solid–fluid reaction can be represented by the following reaction:

$$\mathrm{A(fluid)}+b\mathrm{B(solid)}\rightarrow\mathrm{Products} \quad (5)$$

where A, B and b represented H_2SO_4, magnesiation-roasted vanadium slag and stoichiometric coefficient, respectively.

The acid leaching process of magnesiation-roasted vanadium slag consisted of the following five steps: (1) transport of H_2SO_4 from the bulk solution to the particle surface; (2) diffusion of H_2SO_4 through the solid ash layer from the particle surface to the surface of unreacted core of magnesiation-roasted vanadium slag; (3) reaction between H_2SO_4 and magnesiation-roasted vanadium slag on the surface of the unreacted core; (4) diffusion of the resultant $(VO_2)_2SO_4$ through the solid ash layer from the reaction interface to the particle surface; (5) transport of the resultant $(VO_2)_2SO_4$ from the particle surface to the bulk solution.

Each step above can be the rate-controlling step during the acid leaching process. Their relative integral rate equations were derived and shown in Eqs. (6)−(8) [32]:

If the leaching rate is controlled by the diffusion through solid ash layer, the integral rate equation will be

$$1-3(1-x)^{2/3}+2(1-x)=k_d t \quad (6)$$

If the leaching rate is controlled by the surface chemical reaction, the integral rate equation will be

$$1-3(1-x)^{1/3}=k_r t \quad (7)$$

If the leaching rate is controlled by the diffusion through liquid film, the integral rate equation will be

$$1-(1-x)^{2/3}=k_l t \quad (8)$$

where x and t are the vanadium leaching efficiency and leaching time, respectively; k_d, k_r and k_l are the apparent rate constants for pore diffusion, surface chemical reaction, and liquid film diffusion, respectively.

As shown in Fig. 7, there were two stages in the leaching kinetics of vanadium from magnesiation-roasted vanadium slag. The first stage occurred at the beginning of the acid leaching process (0−10 min) and the second stage occurred after 10 min. Therefore, the leaching kinetics of vanadium was analyzed separately in two stages.

3.3.1 Leaching kinetics in short time stage

The kinetic data for the initial stage (0−10 min) of the acid leaching was fitted with Eqs. (6)−(8) under various conditions. The rate constants and correlation coefficients of regression were listed in Table 2. As shown, the largest regression coefficients were obtained for the regime type of

solid layer diffusion control, indicating that the diffusion through solid ash layer contributed significantly to the leaching rate of vanadium in the initial stage. The rate constant k_d was obtained from slopes in Fig. 8 and ln k_d was plotted against $1/T$ to calculate apparent activation energy (E_a). According to the Arrhenius equation, E_a was calculated to be 20.21 kJ/mol (R^2=0.9908) in the initial stage (Fig. 9). It is commonly known that the activation energy of diffusion-controlled process is typically

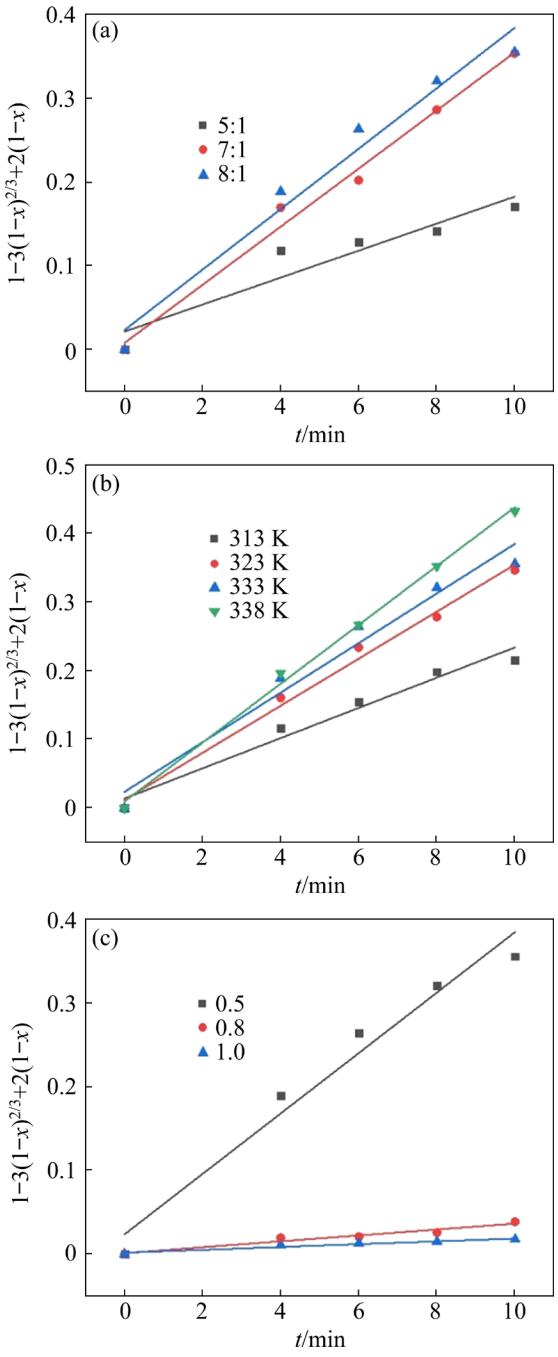

Fig. 8 Plots of $1-3(1-x)^{2/3}+2(1-x)$ vs leaching time (t) at different L/S ratios (a), leaching temperatures (b) and pH values (c)

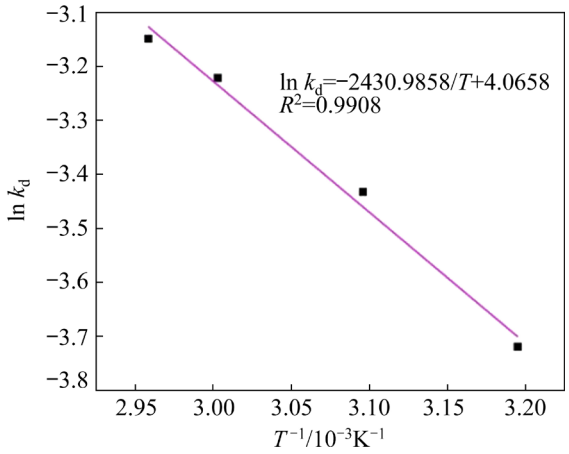

Fig. 9 Arrhenius plot for leaching system (0−10 min)

below 12 kJ/mol while that of chemical-reaction-controlled process is usually above 40 kJ/mol. Thus, the activation energy of process controlled by both diffusion and chemical reactions is usually between 12 and 40 kJ/mol [33]. The calculated E_a (20.21 kJ/mol) was between 12 and 40 kJ/mol, indicating that the leaching rate in the initial stage was controlled by both solid ash layer diffusion and chemical reaction. However, solid layer diffusion contributed more than chemical reaction to the controlling of leaching rate. This was because at the beginning of the leaching process, $MgSiO_3$ reacted with H_2SO_4 to form H_2SiO_3 colloids, which hindered the diffusion of vanadate ions, thereby influencing the reaction kinetics of $Mg_2V_2O_7$ and $Mn_2V_2O_7$ with H_2SO_4. This was also proved by R^2 values of fitting results as shown in the last column in Table 2. To sum up, the leaching rate in the initial stage was controlled by both solid ash layer diffusion and chemical reactions.

3.3.2 Leaching kinetics in long-time stage

Equations (6)−(8) cannot be applied directly to the long-time stage (10−30 min) since the boundary conditions of this stage have changed. Under new boundary conditions Eqs. (6)−(8) were transformed respectively and expressed as follows:

Solid ash layer diffusion control:

$$1-3[(1-x)/(1-x_1)]^{2/3}+2[1-(1-x_1)^{1/3}(x-x_1)]=k_d(t-t_1) \quad (9)$$

Chemical reaction control:

$$1-[(1-x)/(1-x_1)]^{1/3}=k_r(t-t_1) \quad (10)$$

Liquid film diffusion control:

$$1-[(1-x)/(1-x_1)]^{2/3}=k_l(t-t_1) \quad (11)$$

where x_1 is the vanadium extraction efficiency at 10 min, and t_1 is 10 min. Experimental data were fitted into Eqs. (9)−(11) in various conditions. The results were shown in Table 3 and Fig. 10. In Table 3, the largest regression coefficients were obtained for the regime type of chemical reaction control. This proved that the leaching efficiency in the long-time stage was controlled by chemical reactions. This was because when the reaction progressed, the pH value of the liquid was constantly increased, and the chemical reaction rate in the system was lower than mass transfer rate. Thus, the chemical reactions became the rate-controlling step. The E_a value for the long-time stage was calculated by linear regression of $\ln k_r$ against $1/T$ (Fig. 11). The obtained E_a was 40.94 kJ/mol (R^2=0.9912), which was greater than 40 kJ/mol. This confirmed that the leaching process was controlled by the chemical reaction in the stage of 10−30 min.

Table 2 Apparent rate constants for kinetics models and correlation coefficients (0−10 min)

Parameter		Diffusion through liquid film, $1-(1-x)^{2/3}$		Surface chemical reaction, $1-3(1-x)^{1/3}$		Diffusion through solid ash layer, $1-3(1-x)^{2/3}+2(1-x)$	
		k_l	R^2	k_r	R^2	k_d	R^2
L/S ratio	5:1	0.0432	0.7883	0.0249	0.8057	0.0161	0.8927
	7:1	0.0624	0.8932	0.0391	0.9286	0.0347	0.9891
	8:1	0.0635	0.8557	0.0400	0.8917	0.0399	0.9690
Temperature	313 K	0.0505	0.8606	0.0298	0.8855	0.0242	0.9702
	323 K	0.0621	0.8856	0.0388	0.9208	0.0323	0.9903
	333 K	0.0635	0.8557	0.0400	0.8917	0.0399	0.9690
	338 K	0.0688	0.8960	0.0446	0.9379	0.0429	0.9965
pH	0.5	0.0635	0.8557	0.0400	0.8917	0.0399	0.9690
	0.8	0.0208	0.8788	0.0110	0.8867	0.0035	0.9500
	1.0	0.0145	0.8299	0.0075	0.8352	0.0017	0.9418

Table 3 Apparent rate constants for kinetics models and correlation coefficients (10−30 min)

Parameter		Diffusion through liquid film, $1-[(1-x)/(1-x_1)]^{2/3}$		Surface chemical reaction, $1-[(1-x)/(1-x_1)]^{1/3}$		Diffusion through solid ash layer, $1-3[(1-x)/(1-x_1)]^{2/3}+2[1-(1-x_1)^{1/3}(x-x_1)]$	
		k_l	R^2	k_r	R^2	k_d	R^2
L/S ratio	5:1	0.002	0.967	0.001	0.9672	0.0042	0.9667
	7:1	0.0139	0.9491	0.0074	0.9591	0.0367	0.9493
	8:1	0.0197	0.9663	0.0098	0.9867	0.0522	0.9648
Temperature	313 K	0.007	0.9612	0.0036	0.9641	0.0362	0.9641
	323 K	0.0106	0.9494	0.0056	0.9503	0.0277	0.9496
	333 K	0.0197	0.9663	0.0098	0.9867	0.0522	0.9648
	338 K	0.0196	0.9901	0.011	0.9904	0.054	0.9899
pH	0.5	0.0197	0.9663	0.0098	0.9867	0.0522	0.9648
	0.8	0.0028	0.852	0.0015	0.8675	0.0034	0.8558
	1.0	0.0023	0.8278	0.0012	0.8344	0.002	0.8335

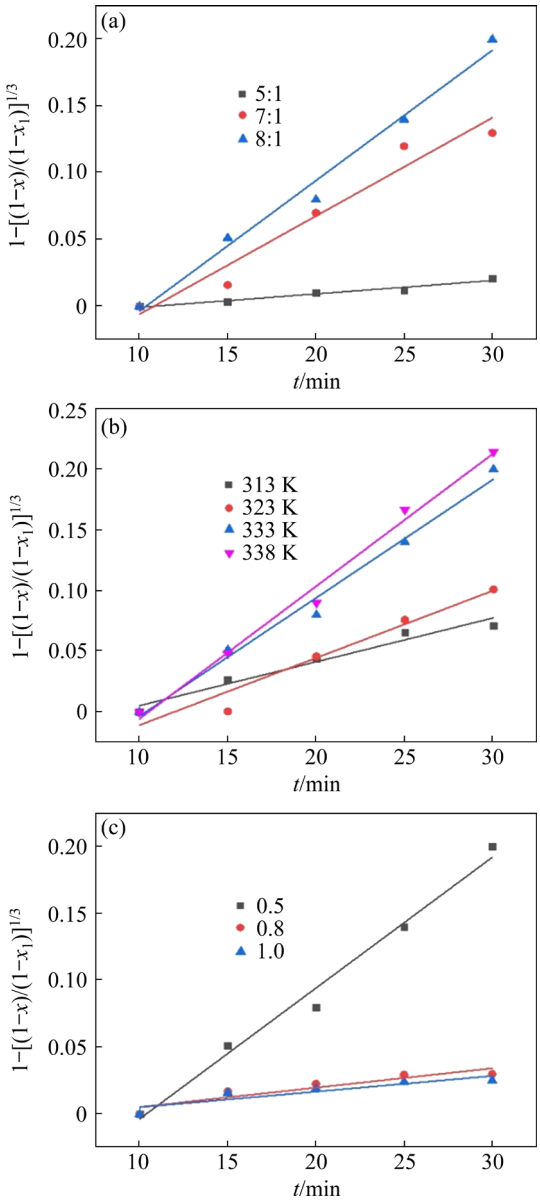

Fig. 10 Plots of $1-[(1-x)/(1-x_1)]^{1/3}$ vs leaching time (t) at different L/S ratios (a), leaching temperatures (b) and pH values (c)

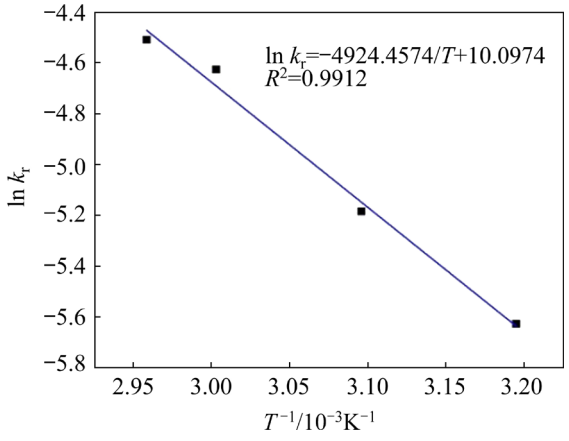

Fig. 11 Arrhenius plot for leaching system (10−30 min)

4 Conclusions

(1) During the acid leaching process, the $MgSiO_3$ and most vanadates reacted with the sulfuric acid in the initial 10 min, and the remaining vanadates reacted with the sulfuric acid within the following 20 min. V in the leaching liquid existed in the form of V^{5+}, while Fe did not enter the leaching liquid during the whole leaching process.

(2) The influences of leaching conditions on vanadium leaching kinetics were systematically investigated. The acid leaching proceeded as two stages, namely the initial stage of 0−10 min and the long-time stage of 10−30 min. In the initial stage, the leaching efficiency increased sharply, while the leaching efficiency increased gradually at the long-time stage.

(3) Kinetic studies showed that the acid leaching kinetics followed the SCM. In the short time stage of the acid leaching, both solid layer diffusion and chemical reactions contributed to the control of leaching rate. The leaching rate in the long-time stage was controlled by the chemical reactions.

CRediT authorship contribution statement

Jie CHENG: Methodology, Investigation, Writing − Original draft; **Hong-yi LI:** Conceptualization, Methodology, Writing − Review & editing, Funding acquisition; **Dong HAI:** Investigation, Data curation; **Xin-mian CHEN:** Visualization, Investigation; **Jiang DIAO:** Project administration; **Bing XIE**: Resources.

Declaration of competing interest

The authors declare that they have no known competing financial interests or personal relationships that could have appeared to influence the work reported in this paper.

Acknowledgments

The authors are grateful for the financial supports from the National Natural Science Foundation of China (Nos. 52074050, 52222407).

References

[1] LI Hong-yi, CHENG Jie, WANG Cheng-jie, SHEN Shuo, DIAO Jiang, XIE Bing. Ecofriendly selective extraction of vanadium from vanadium slag with high chromium content via magnesiation roasting−acid leaching [J]. Metallurgical and Materials Transactions B, 2022, 53: 604−616.

[2] LI Hong-yi, WANG Kang, WANG Cheng-jie, LIN Min-min, XIE Bing. Atomic atmosphere: A way to understand phase evolution during vanadium slag roasting at the atomic level [J]. Acta Crystallographica, 2019, 75: 927−932.

[3] LI Hong-yi, CHEN Xin-mian, LI Dan-qing, GUO Yun, DIAO Jiang, XIE Bing. Quick valence analysis method of vanadium toward accurate toxicity assessment of vanadium-containing hazardous wastes [J]. Transactions of Nonferrous Metals Society of China, 2021, 31: 3602−3612.

[4] WEN Jing, JIANG Tao, XU Ying-zhe, LIU Jia-yi, XUE Xiang-xin. Efficient separation and extraction of vanadium and chromium in high chromium vanadium slag by selective two-stage roasting-leaching [J]. Metallurgical and Materials Transactions B, 2018, 49: 1471−1481.

[5] LIANG Xing, GAO Guo-hua, LIU Yin-dan, ZHANG Tian-qi, WU Guang-ming. Synthesis and characterization of Fe-doped vanadium oxide nanorods and their electrochemical performance [J]. Journal of Alloys and Compounds, 2017, 715: 374−383.

[6] LI Hong-yi, WANG Cheng-jie, YUAN Yi-heng, GUO Yun, DIAO Jiang, XIE Bing. Magnesiation roasting−acid leaching: A zero-discharge method for vanadium extraction from vanadium slag [J]. Journal of Cleaner Production, 2020, 260: 121091.

[7] LEE J C, KIM E Y, CHUNG K W, KIM R, JEON H S. A review on the metallurgical recycling of vanadium from slags: Towards a sustainable vanadium production [J]. Journal of Materials Research and Technology, 2021, 12: 343−364.

[8] GUO Yun, LI Hong-yi, YUAN Yi-heng, HUANG Jie, DIAO Jiang, LI Gang, XIE Bing. Microemulsion leaching of vanadium from sodium-roasted vanadium slag by fusion of leaching and extraction processes [J]. International Journal of Minerals, Metallurgy and Materials, 2021, 28: 974−980.

[9] CHENG Jie, WANG Cheng-jie, SHEN Shuo, DIAO Jiang, XIE Bing, LI Hong-yi. Synthesis and solubility behavior of magnesium ortho-, meta-, and pyrovanadates [J]. JOM, 2022, 74: 23−29.

[10] WANG Shuai, GUO Yu-feng, ZHENG Fu-qiang, CHEN Feng, YANG Ling-zhi, JIANG Tao, QIU Guan-zhou. Behavior of vanadium during reduction and smelting of vanadium titanomagnetite metallized pellets [J]. Transactions of Nonferrous Metals Society of China, 2020, 30: 1687−1696.

[11] SONG Wen-chen, LI Hong, ZHU Fu-xing, LI Kun, ZHENG Quan. Extraction of vanadium from molten vanadium bearing slag by oxidation with pure oxygen in the presence of CaO [J]. Transactions of Nonferrous Metals Society of China, 2014, 24: 2687−2694.

[12] LIU Hui-bin, DU Hao, WANG Da-wei, WANG Shao-na, ZHENG Shi-li, ZHANG Yi. Kinetics analysis of decomposition of vanadium slag by KOH sub-molten salt method [J]. Transactions of Nonferrous Metals Society of China, 2013, 23: 1489−1500.

[13] ZHANG Ju-hua, ZHANG Wei, ZHANG Li, GU Song-qing. Mechanism of vanadium slag roasting with calcium oxide [J]. International Journal of Mineral Processing, 2015, 138: 20−29.

[14] JIANG Tao, WEN Jing, ZHOU Mi, XUE Xiang-xin. Phase evolutions, microstructure and reaction mechanism during calcification roasting of high chromium vanadium slag [J]. Journal of Alloys and Compounds, 2018, 742: 402−412.

[15] LIU Shu-gen, DING Er-mao, NING Ping, XIE Gang, YANG Ni. Vanadium extraction from roasted vanadium-bearing steel slag via pressure acid leaching [J]. Journal of Environmental Chemical Engineering, 2021, 9: 105195.

[16] van VUUREN C P J, STANDER P P. The oxidation of FeV_2O_4 by oxygen in a sodium carbonate mixture [J]. Minerals Engineering, 2001, 14: 803−808.

[17] YU Tang-xia, JIANG Tao, WEN Jing, SUN Hong-yan, LI Ming, PENG Yi. Effect of chemical composition on the element distribution, phase composition and calcification roasting process of vanadium slag [J]. International Journal of Minerals, Metallurgy and Materials, 2022, 29: 2144−2151.

[18] LIU Shi-yuan, ZHEN Yu-lan, HE Xiao-bo, WANG Li-jun, CHOU Kuo-chih. Recovery and separation of Fe and Mn from simulated chlorinated vanadium slag by molten salt electrolysis [J]. International Journal of Minerals, Metallurgy and Materials, 2020, 27: 1678−1686.

[19] YANG Zhao, LI Hong-yi, YIN Xu-chen, YAN Zhi-ming, YAN Xiao-man, XIE Bing. Leaching kinetics of calcification roasted vanadium slag with high CaO content by sulfuric acid [J]. International Journal of Mineral Processing, 2014, 133: 105−111.

[20] WEN Jing, JIANG Tao, LIU Ya-jing, XUE Xiang-xin. Extraction behavior of vanadium and chromium by calcification roasting-acid leaching from high chromium vanadium slag: Optimization using response surface methodology [J]. Mineral Processing and Extractive Metallurgy Review, 2019, 40: 56−66.

[21] WEN Jing, JIANG Tao, ZHOU Wan-ying, GAO Hui-yang, XUE Xiang-xin. A cleaner and efficient process for extraction of vanadium from high chromium vanadium slag: Leaching in $(NH_4)_2SO_4$−H_2SO_4 synergistic system and NH_4^+ recycle [J]. Separation and Purification Technology, 2019, 216: 126−135.

[22] WEN Jing, JIANG Tao, GAO Hui-yang, ZHOU Wan-ying, XU Ying-zhe, ZHENG Xiao-le, LIU Ya-jing, XUE Xiang-xin. An efficient utilization of chromium-containing vanadium tailings: Extraction of chromium by soda roasting−water leaching and preparation of chromium oxide [J]. Journal of Environmental Management, 2019, 244: 119−126.

[23] AARABI-KARASGANI M, RASHCHI F, MOSTOUFI N, VAHIDI E. Leaching of vanadium from LD converter slag using sulfuric acid [J]. Hydrometallurgy, 2010, 102: 14−21.

[24] PENG Hao, GUO Jing, ZHENG Xiao-gang, LIU Zuo-hua, TAO Chang-yuan. Leaching kinetics of vanadium from calcification roasting converter vanadium slag in acidic medium [J]. Journal of Environmental Chemical Engineering, 2018, 6: 5119−5124.

[25] LI Meng, LIU Biao, ZHENG Shi-li, WANG Shao-na, DU Hao, DREISINGER D B, ZHANG Yi. A cleaner vanadium extraction method featuring non-salt roasting and ammonium bicarbonate leaching [J]. Journal of Cleaner Production, 2017, 149: 206−217.

[26] IZCI E. Structural and spectroscopic properties of $MgTi_2O_5$/$MgTiO_3$ composite by solid state technique [J]. Microscopy and Microanalysis, 2013, 19(Suppl.): 1974−1975.
[27] SONG S, CHO H B, KIM H T. Surfactant-free synthesis of high surface area silica nanoparticles derived from rice husks by employing the Taguchi approach [J]. Journal of Industrial and Engineering Chemistry, 2018, 61: 281−287.
[28] TAN B J, KLABUNDE K J, SHERWOOD P M A. X-ray photoelectron spectroscopy studies of solvated metal atom dispersed catalysts. Monometallic iron and bimetallic iron-cobalt particles on alumina [J]. Chemistry of Materials, 1990, 2: 186−191.
[29] SETHI D, JADA N, KUMAR R, RAMASAMY S, PANDEY S, DAS T, KALIDOSS J, MUKHERJEE P S, TIWARI A. Synthesis and characterization of titania nanorods from ilmenite for photocatalytic annihilation of *E. coli* [J]. Journal of Photochemistry and Photobiology B, 2014, 140: 69−78.
[30] BEAMSON G, MOSLEMZADEH N, WEIGHTMAN P, WATTS J F, PHENOMENA R. AlK_α and $CuK_{\alpha1}$ excited XPS of vanadium oxide and VF_3 powders: Measurement of the V 1s – KLL Auger parameters [J]. Journal of Electron Spectroscopy and Related Phenomena, 2008, 162: 19−24.
[31] ALONSO B, LIVAGE J. Synthesis of vanadium oxide gels from peroxovanadic acid solutions: A ^{51}V NMR study [J]. Journal of Solid State Chemistry, 1999, 148: 16−19.
[32] ABDEL-AAL E A, RASHAD M M. Kinetic study on the leaching of spent nickel oxide catalyst with sulfuric acid [J]. Hydrometallurgy, 2004, 74: 189−194.
[33] ASHRAF M, ZAFAR Z I, ANSARI T M. Selective leaching kinetics and upgrading of low-grade calcareous phosphate rock in succinic acid [J]. Hydrometallurgy, 2005, 80: 286−292.

镁化焙烧钒渣中钒的酸浸动力学研究

成 洁[1]，李鸿义[1,2]，海 栋[1]，陈新勉[1]，刁 江[1,2]，谢 兵[1]

1. 重庆大学 材料科学与工程学院，重庆 400044；
2. 重庆大学 国家镁合金材料工程技术研究中心，重庆 400044

摘 要：为了促进钒渣镁化焙烧−酸浸提钒法的工业应用，研究钒渣镁化焙烧熟料中钒的酸浸出动力学。结合XRD、XPS 和 SEM，揭示在浸出初期的 10 min 内，$MgSiO_3$ 和大部分钒酸盐急剧地消耗酸，形成 SiO_2 和 V(V)的氧钒根离子。通过研究钒浸出效率随浸出时间的变化，建立钒浸出的动力学模型。结果表明，浸出过程分为两个不同的阶段，且两个阶段的动力学均遵循收缩核模型。0~10 min 的浸出速率由固体产物层扩散和化学反应共同控制，而 10~30 min 的浸出速率仅由化学反应控制。因此，浸出初始 10 min 内加速传质很关键，而后续 20 min 内精确控温至关重要。

关键词：浸出动力学；镁化焙烧；酸浸；钒提取；钒渣

(Edited by Wei-ping CHEN)